Comparing Field Emission Stability of Lithography-free, Modified Multi-Walled Carbon Nanotubes

Archana Pandey, Abhishek Prasad, Jason Moscatello, and Yoke Khin Yap

Department of Physics, Michigan Technological University, Houghton, MI 49931, U.S.A.

ABSTRACT

Field emission from carbon nanotubes (CNTs) has been known for more than a decade but there is no commercialized product available in the market. Apparently, we need to improve our basics understanding on stable field emission from CNTs. Here we compared the field emission properties of as grown vertically-aligned multi-walled carbon nanotubes (MWCNTs) to two types of modified MWCNTs: 1) Conical bundles of opened-tip MWCNTs, and 2) Opened-tip MWCNTs embedded in poly-methyl methacrylate (PMMA). We found that both types of modified MWCNTs have lower emission thresholds and better emission stability than the as grown samples. Among these modified samples, MCNTs embedded in PMMA has lower emission thresholds and better emission stability. We attributed these improvements to the filling of spacing between MWCNTs with PMMA that has higher dielectric constant than vacuum.

INTRODUCTION

Tremendous efforts have been evidenced on the study of electron field emission from carbon nanotubes (CNTs). Although this property has been known for more than a decade [1], commercial field emission products based on CNTs is still not available. The possible reason for this situation is that the basic science for stable field emission still requires further investigation. Research efforts reported so far focused mainly on the low emission threshold fields (E_{th}) of various types of CNTs and the design of device configurations. However, long term emission stability, for example continuous emission test for more than 10 hours, has not been sufficiently discussed [2-8].

We have focused our efforts in understanding basic factors that contribute towards stable field emission from CNTs. We found that graphitic order of CNTs is one of the key factors for stable emission [9, 10]. In the present paper, we describe the methodology to increase the long term emission stability from multiwalled carbon nanotubes (MWCNTs) while keeping the emission threshold electric field low.

We have found two simple and effective techniques for improving field emission stability of vertically-aligned MWCNTs without involving lithography processes:

1) self-assembled conical bundles of opened-tip VA-MWCNTs,
2) Opened-tip VA-MWCNTs embedded in poly-methyl methacrylate (PMMA).

The opened-tip conical nanotube bundles were prepared by acid etching of the residual Ni catalysts at the tips of as grown VA-MWCNTs. The etched samples will self-assembled in to regular arrays of conical bundles. The PMMA embedded samples were prepared by dip-coating

of the as-grown VA-MWCNTs with PMMA followed by mechanical polishing to expose the tips of these VA-MWCNTs. All these samples were then compared for their current density versus applied electric field (*J-E*) properties, long-term emission stability for continuous emission, as well as their emission site densities, in a high-vacuum chamber (x10^{-7} mbar) [9].

We found that both the emission threshold field and stability were improved for both types of modified samples. The threshold electric field (E_{th}) is defined as the electric field required for emitting electrons to a level of 1 μA/cm^2. For the as grow samples, E_{th} was ~4.4 V/μm. This threshold field was reduced to 3.14 V/μm for the opened-tip, conical nanotube bundles. The PMMA coated samples have the lowest emission threshold (E_{th} = 2.88 V/μm). In addition, the PMMA-embedded sample showed a significant improvement in emission stability as compared to the as-grown and opened-tip conical bundled CNT samples.

EXPERIMENTAL DETAILS

All the MWCNT samples used in this experiment were grown by dual RF-plasma-enhanced chemical vapor deposition (PECVD). The detailed experimental procedures were reported elsewhere [10]. In brief, Ni films (10 nm thick) were first deposited on *p*-type Si substrates (1–10 Ω cm) by RF magnetron sputtering. These substrates were then used for the growth of VA-MWCNTs at 450^{0}C by using pure methane gas. Our VA-MWCNTs were grown within a circular area (7mm in diameter). Three identical samples can be prepared in each growth process.

The conical bundles of opened-tip VA-MWCNTs are prepared as follows. First, the residual Ni catalytic nanoparticles at the tips of the as grown VA-MWCNTs were removed by etching in HNO$_3$ acid (70 vol.%, for 5 min). Then, the etched samples were rinsed with de-ionized water and toluene. We found that the VA-MWCNTs will self-organize into arrays of conical bundles. These processes lead to catalyst-free opened-tip conical bundled MWCNTs.

The sample preparation procedure for the opened-tip VA-MWCNT samples embedded in PMMA is summarized in Figure 1. First, PMMA solution was prepared by adding the developer solution to a volume ratio of 1:1. Then, an as grown VA-MWCNT sample (Figure 1a) was dipped into the solution for 15 minutes before removal. This was followed by annealing the sample at ~100°C for 2-3 minutes to dry the sample (Figure 1b). Finally, the sample was mechanically polished by using fiber-free lapping cloth and a colloidal silica (0.02 μm) solution to expose the tips of carbon nanotubes. VA-MWCNTs with the exposed tips, spatially separated by PMMA dielectric is schematically shown in Figure 1c. These samples were then ready for field emission test measurements.
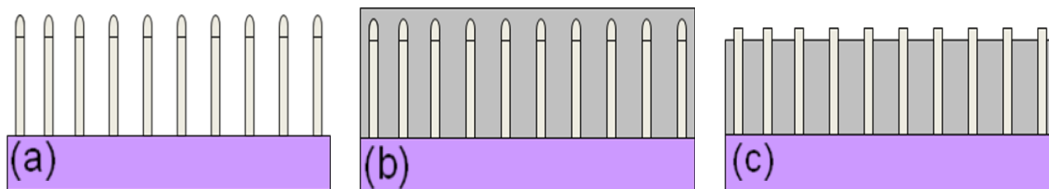

Figure 1. Fabrication steps of opened-tip VA-MWCNT embedded in PMMA. (a) As grown VA-MWCNTs on Si substrates (b) Dip coating of VA-MWCNTs by PMMA and (c) Mechanical polishing to open the tips of CNTs.

DISCUSSION

The field emission characteristic curve for the as grown VA-MWCNTs is shown in Figure 2a. This is the current density (J) versus the applied electric field (E) characteristics of the sample. The Fowler–Nordheim (F-N) equation [11-12], $J = A\beta^2 E^2 \ exp(-B\Phi^{3/2}/\beta E)$ is used to describe field emission, where A, B are constants, E is the applied electric field in V cm^{-1}, and Φ is the work function in eV, β is the field enhancement factor.
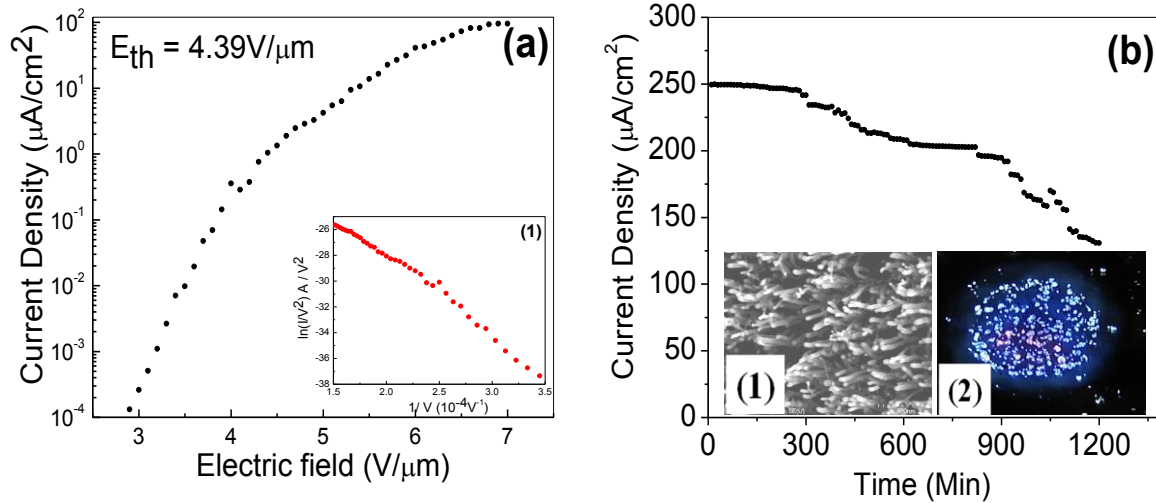

Figure 2. (a) The field emission J-E curve for the as grown VA-MWCNTs and the corresponding F-N plot (inset 1). (b) The corresponding emission stability curve, SEM images of the sample (inset 1), and images of the emission sites (inset 2).

A linear F-N plot (inset 1 of Figure 2a) verified that the detected currents are due to quantum tunneling. The threshold electric field, E_{th} is estimated as 4.39 V/μm for the as grown sample. Figure 2b describes the field emission stability of the as grown sample. The SEM images of the sample are shown as the inset 1 of Figure 2b. As shown from the plot, the emission from the as grown sample is not stable after ~300 min (five hours) of continuous emission. Inset 2 of Figure 2b shows the images of the emission sites as observed on the ITO electrode (anode). As shown, the pattern resembles the circular area of the VA-MWCNT film.

We have then tested the conical bundles of opened-tip VA-MWCNTs to understand the effect of the etching and bundling. As shown in Figure 3a, $E_{th} = 3.82$ V/μm are detected from the etched and bundled samples. The linear F-N relations (inset 1 of Figure 3a) were also revealed. As previously shown in inset 1 of Figure 2b, the distances between the as grown VA-MWCNTs are small (50–300 nm) and will initiate screening effect that reduced the β factors. This means not all the as grown VAMWCNTs will contribute to the collected current except those are longer in lengths or located at the edges of the larger spacing. For the etched and bundled sample shown in inset 1 of Figure 3b, the distances between bundles are more than one micrometer and thus will have less screening effect [11].

Thus, each bundle can be considered as a larger emission pyramid. We think that this has contributed to the reduced E_{th} detected here. We have compared this sample for its emission

stability. As shown in Figure 3b, the etched and bundled sample is stabilized at a current density >180 µA/cm^2 after continuous 20-h operation while the as grown sample has reduced its current density to <125 µA/cm^2 (Figure 2b). As shown in the insets of Figure 3b, the emission density for the etched and bundled sample (inset 2) is higher than that of the as grown sample (inset 2 in Figure 2b). Apparently, lower screening effects on the bundled sample offers more emission sites. Since the emission loads (heat and mechanical stress from Joule heating) is now shared by more emission sites, the emission stability is thus improved. As indicated by the FN equation, a lower local field on each emitter will lead to the emission of lower current density per emitter. This will reduced Joule heating and stresses on these emitters and thus produce stable emission.
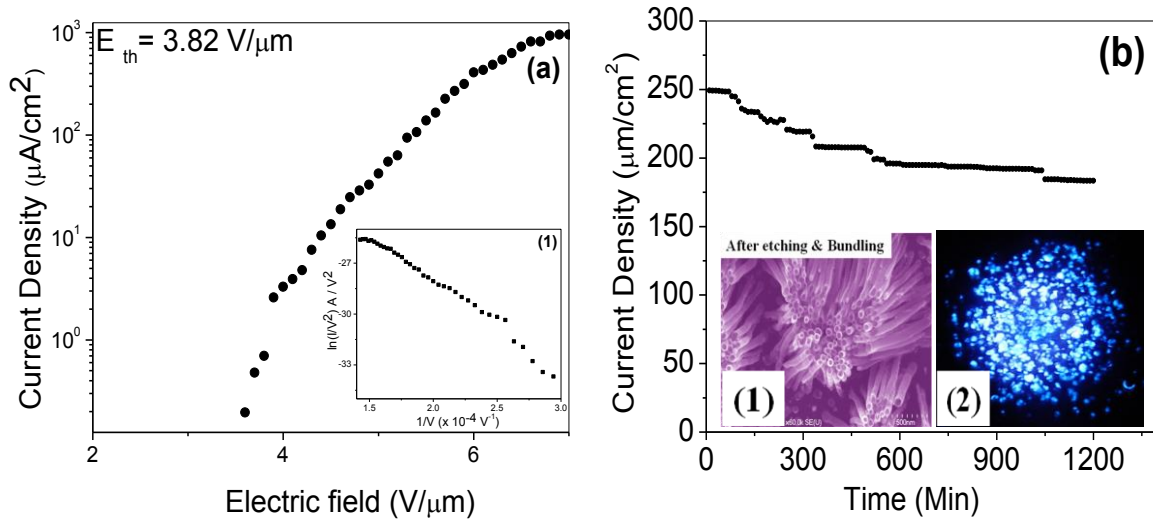

Figure 3. (a) The field emission *J-E* curve for the etched and bundled MWCNTs and the corresponding F-N plot (inset 1). (b) The corresponding emission stability curve, SEM images (inset 1) and images of the emission sites (inset 2).

Next we have examined the emission properties of samples embedded in PMMA. As can be seen from Figure 4a, E_{th} for the PMMA embedded samples was much lower (2.71V/µm) as compared to that for the opened-tip conical bundles and the as grown VA-MWCNTs. The threshold electric field depends on various factors. Here two of the following are in consideration: the aspect ratio of the CNTs and their inter-tube spacing. High aspect ratio of carbon nanotubes enables large electric enhancement at the tips and initiates electron emission at a relatively lower applied electric field. All of our samples, as-grown as well as PMMA-embedded samples, were grown simultaneously under the same growth conditions, so they have the same length and diameter and, therefore, same aspect ratio. This was confirmed by SEM observation (not shown). So in our case, the lower threshold field detected for the PMMA-coated sample cannot be due to variations in the CNT aspect ratios and the inter-tube spacing. Obviously, the only difference between the as grown VA-MWCNTs and PMMA-embedded VA-MWCNTs is in the dielectric filling (PMMA) between each individual VA-MWCNTs. Tentatively, we think that the dielectric properties of PMMA has helped to reduce the screening effect between the CNTs and to improve the field emission performance.

Figure 4b shows the emission stability plot for the PMMA-coated MWCNT sample. It can be clearly seen that the stability after PMMA coating improves considerably than that for the as-grown and etched and bundled samples. As both of the samples have MWCNTs with same aspect ratio, same structural order, and same inter-tube spacing, we think that the improvement in the emission stability of the PMMA-coated VA-MWCNTs sample is partly due to the reduction in the screening effect. Further study is required to understand the actual reasons for the improvement.
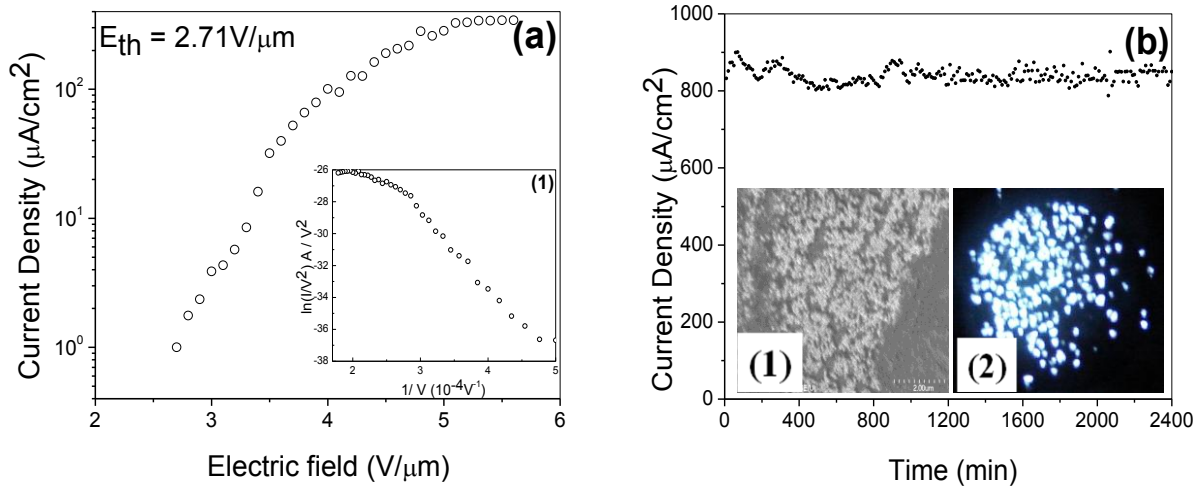

Figure 4. (a) The field emission *J-E* curve for the PMMA coated VA-MWCNTs and the corresponding F-N plot (inset 1). (b) The corresponding emission stability curve, SEM images of the exposed CNT tips (inset 1) and images of the emission sites (inset 2).

CONCLUSIONS

In summary, we found that opened-tip conical bundles of MWCNTs can produce more stable electron emission than the as grown samples. Bundling of these VA-MWCNTs can reduce the screening effects, increase the emission density, and improve the emission stability. We also demonstrated a significant improvement in the field emission stability in the VA-MWCNT film embedded in PMMA. The threshold field to emit electrons at a level of 1 $\mu A/cm^2$ was reduced to 2.71 V/μm for the PMMA embedded sample as compared 4.39 V/μm of the as grown VA-MWCNTs. We discussed the possible reasoning behind this field emission improvement and attributed this to the reduction in the screening effect from the neighboring MWCNTs due to the higher dielectric properties of PMMA.

ACKNOWLEDGMENTS

REFERENCES

1. A. G. Rinzler, J. H. Hafner, P. Nikolaev, L. Lou, S. G. Kim, D. Tomanek, P. Nordlander, D. T. Colbert and R. E. Smalley, *Science* **269**, 1550 (1995).
2. L. Nilsson, O. Groening, C. Emmenegger, O. Kuettel, E. Schaller, L. Schlapbach, *Appl Phys Lett* **76**, 2071 (2000).
3. W.A. deHeer, A. Chatelain, D. Ugarte, *Science* **270**, 1179 (1995).
4. P.G. Collins, A. Zettl, *Appl Phys Lett* **69**, 1969 (1996).
5. W.B. Choi, D.S. Chung, J.H. Kang, H.Y. Kim, Y.W. Jin, I.T. Han, *Appl Phys Lett* **75:3**, 129 (1999).
6. Y. Saito, K. Hamaguchi, S. Uemura, K. Uchida, Y. Tasaka, F. Ikazaki, *Appl Phys* **A67**, 95 (1998).
7. J.M. Bonard, J.P. Salvetat, T. Stockli, L. Forro, A. Chatelain, *Appl Phys* **A69**, 245 (1999).
8. J.M. Bonard, H. Kind, T. Stockli, L.O. Nilsson, *Solid-State Electron* **45**, 893 (2001).
9. B. Ulmen, V. K. Kayastha, A. DeConinck, J. Wang, and Y. K. Yap, *Diamond and Related Materials* **15**, 212 (2006).
10. V. K. Kayastha, B. Ulmen and Yoke Khin Yap, *Nanotechnology* **18**, 035206 (2007).
11. A. Pandey, A. Prasad, J. Moscatello, B. Ulmen, Y. K. Yap, *Carbon* **48**, 287 (2010).
12. R. H. Fowler and L. Northeim, *Proc. R. Soc.* A **119,** 173 (1928).